GEOLOGY | THE GEOLOGICAL SOCIETY OF AMERICA®

https://doi.org/10.1130/G48795.1

Manuscript received 6 January 2021
Revised manuscript received 17 March 2021
Manuscript accepted 26 March 2021

Published online 19 May 2021

Pace, magnitude, and nature of terrestrial climate change through the end-Permian extinction in southeastern Gondwana

T.D. Frank[1]*, C.R. Fielding[1], A.M.E. Winguth[2], K. Savatic[1], A. Tevyaw[1], C. Winguth[2], S. McLoughlin[3], V. Vajda[3], C. Mays[3], R. Nicoll[4], M. Bocking[5] and J.L. Crowley[6]

[1]Department of Earth and Atmospheric Sciences, University of Nebraska–Lincoln, 126 Bessey Hall, Lincoln, Nebraska 68588-0340, USA
[2]Department of Earth and Environmental Sciences, University of Texas Arlington, 107 Geoscience Building, 500 Yates Street, Arlington, Texas 76019, USA
[3]Department of Palaeobiology, Swedish Museum of Natural History, Box 50007, S-104 05 Stockholm, Sweden
[4]72 Ellendon Street, Bungendore, NSW 2621, Australia
[5]Bocking Associates, 8 Tahlee Close, Castle Hill, NSW 2154, Australia
[6]Isotope Geology Laboratory, Boise State University, 1910 University Drive, Boise, Idaho 83725-1535, USA

ABSTRACT

Rapid climate change was a major contributor to the end-Permian extinction (EPE). Although well constrained for the marine realm, relatively few records document the pace, nature, and magnitude of climate change across the EPE in terrestrial environments. We generated proxy records for chemical weathering and land surface temperature from continental margin deposits of the high-latitude southeastern margin of Gondwana. Regional climate simulations provide additional context. Results show that *Glossopteris* forest-mire ecosystems collapsed during a pulse of intense chemical weathering and peak warmth, which capped ~1 m.y. of gradual warming and intensification of seasonality. Erosion resulting from loss of vegetation was short lived in the low-relief landscape. Earliest Triassic climate was ~10–14 °C warmer than the late Lopingian and landscapes were no longer persistently wet. Aridification, commonly linked to the EPE, developed gradually, facilitating the persistence of refugia for moisture-loving terrestrial groups.

INTRODUCTION

The end-Permian extinction (EPE), the most severe biotic crisis of the Phanerozoic (Wignall, 2015), led to the fundamental restructuring of terrestrial and marine ecosystems. The consensus view is that the EPE occurred as a consequence of Siberian Traps volcanism, which generated large volumes of sulfate aerosols and CO_2 over a short interval (Burgess et al., 2017), with further contributions of greenhouse gases attributed to thermal metamorphism of Siberian coal measures (Retallack and Jahren, 2008). Although the direct causes of the terrestrial extinction are still debated, the marine extinction is linked to ocean acidification and deoxygenation (Wignall and Twitchett, 1996; Kump et al., 2005; Knoll et al., 2007; Riccardi et al., 2007). Questions remain about relationships between extinctions on land and in the ocean, with some arguing that the devastation of terrestrial plant communities played a pivotal role in the marine extinction (Algeo and Twitchett, 2010; Benton and Newell, 2014; Kaiho et al., 2016; Sun et al., 2018). Understanding such relationships requires constraining the timing and nature of environmental changes surrounding the terrestrial extinction in various basin settings and paleolatitudes.

Among the few quantitative paleoclimate proxies applicable to terrestrial successions are those related to chemical weathering (Cao et al., 2019), a process that intensifies with increasing warmth and humidity (Martini and Chesworth, 2013). The chemical index of alteration (CIA; Nesbitt and Young, 1982) traces the conversion of feldspars to clay minerals via hydration during the weathering of fine-grained siliciclastics, providing insights into temporal changes in chemical weathering and climate. Li and Yang (2010) showed that CIA values derived from suspended sediment in modern large rivers are, at the global scale, particularly sensitive to land surface temperature (LST), latitude at the river mouth, and soil depth in drainage basins. Yang et al. (2014) quantified relationships between the CIA and LST, providing a paleothermometer.

In this study, we apply the CIA and LST proxies to examine changes in weathering intensity and temperature across the terrestrial EPE along a temperate to subpolar continental margin (Fig. 1). Results are interpreted within the context of sedimentological and paleofloral observations from the same sections and compared to regional climate change results provided by the Community Climate System Model (CCSM3.0; Collins et al., 2006; Winguth et al., 2015; https://www.cesm.ucar.edu/models/ccsm3.0/) for the late Permian and Early Triassic.

STUDY AREA

We examined seven cores through Permian and Triassic continental margin deposits preserved in the Bowen-Gunnedah-Sydney Basin System (BGSBS), a narrow composite basin that stretched from ~55° to 65°S paleolatitude along the eastern margin of present-day Australia (Fig. 1B). This succession accumulated in a retroarc foreland basin setting associated with the late Permian–Triassic Hunter-Bowen orogeny (Holcombe et al., 1997). A continental volcanic arc produced numerous zircon-bearing tuff beds, which provide a framework for high-resolution radiogenic isotope ages via chemical abrasion–isotope dilution–thermal ionization mass spectrometry (Metcalfe et al., 2015; Fielding et al., 2019, 2021; McLoughlin et al., 2021). Four drill cores—Geological Survey of Queensland (GSQ) Emerald New Series 7 (ENS7), GSQ Springsure 19 (SS19), GSQ Taroom 10 (T10), and Origin Energy Meeleebee 5 (MEE5)—constitute a north-south transect through the Bowen Basin

*E-mail: tfrank2@unl.edu

CITATION: Frank, T.D., et al., 2021, Pace, magnitude, and nature of terrestrial climate change through the end-Permian extinction in southeastern Gondwana: Geology, v. 49, p. 1089–1095, https://doi.org/10.1130/G48795.1

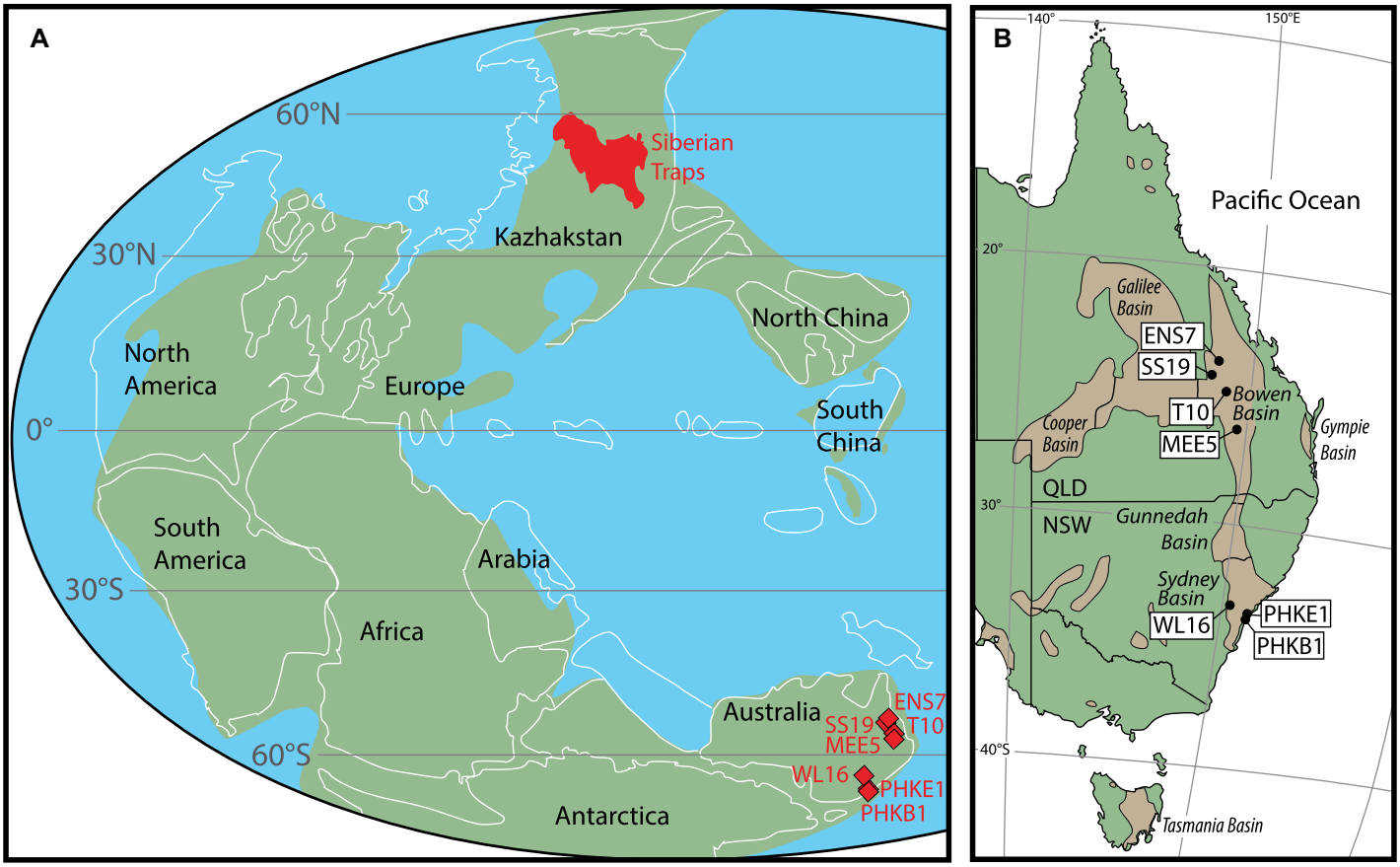

Figure 1. Location maps showing late Permian–Early Triassic paleogeography with drill-core paleolocations marked (A) and present-day locations of boreholes in Permian-Triassic basins in eastern Australia (B). QLD—Queensland; NSW—New South Wales.

(Fig. 2). In the Sydney Basin, drill core Wancol Lithgow DDH16 (WL16) is located at the western cratonic margin, and Pacific Power Hawkesbury Bunnerong DDH1 (PHKB1) and Eveleigh DDH1 (PHKE1) were drilled in the basin axis (Fig. 2). Core locations and data are provided in the Supplemental Material[1].

Lopingian pre-EPE strata of the BGSBS record alluvial and coastal plain environments, with erosionally based, cross-bedded sandstone bodies indicative of fluvial channels, and interbedded coal seams and siltstones containing a rich *Glossopteris* flora, which records flood basins and forested mires (Fielding et al., 2019, 2021). Here, the EPE is marked by the abrupt disappearance of Permian forest-mire communities and the end of peat deposition (Michaelsen, 2002; Fielding et al., 2019; Vajda et al., 2020; McLoughlin et al., 2021), which, in combination with the spore-pollen biostratigraphy (McKellar, 1977; Mays et al., 2020), provides a datum for regional correlation (Fig. 2). In the studied cores, the extinction horizon is conformably overlain by as much as 5 m of mudrock-dominated strata (Fig. 3). Lower Triassic strata record the continuation of depositional environments similar to those characterizing the Lopingian but lacking coal and showing evidence of increasingly well-drained conditions (Fielding et al., 2019, 2021).

METHODS

We used molar concentrations of major element oxides in mudrocks, determined via X-ray fluorescence, to calculate CIA values as follows:

$$\mathrm{CIA} = 100 \times \frac{\mathrm{Al_2O_3}}{\mathrm{Al_2O_3} + \mathrm{CaO^*} + \mathrm{K_2O} + \mathrm{Na_2O}}, \quad (1)$$

where CaO* represents silica-bound Ca. Unweathered crystalline source rocks are characterized by low CIA values (45–55). With progressive weathering and loss of mobile elements, values approach 100. As detailed in the Supplemental Material, samples were screened to assess the influence of factors unrelated to weathering on the CIA, such as changes in provenance, hydraulic sorting, and diagenesis. Elemental ratios and petrography showed no changes in provenance (Tables S1 and S2 in the Supplemental Material). However, some (mainly pre-EPE) samples were affected by K metasomatism (Figs. S2–S4, Table S1). CIA values of affected samples were corrected using the approach of Panahi et al. (2000). Both CIA and corrected ($\mathrm{CIA_{corr}}$) values are presented (Figs. 2 and 3). LSTs are estimated using the equation developed by Yang et al. (2014):

$$\mathrm{LST(°C)} = 0.56 \times \mathrm{CIA} - 25.7 \ (r^2 = 0.50). \quad (2)$$

With an uncertainty of ~±5 °C, the relationship is robust over a CIA range of ~50–90, corresponding to 3–25 °C. LST records were smoothed using a two-point moving average to reflect time-averaged conditions at each location while accounting for variability in sampling resolution. The CCSM3.0 was used to simulate surface air temperature (SAT) and precipitation at the paleolocation of the BGSBS (Fig. 4). Tabulated data and further details on analytical methods and climate modeling are provided in the Supplemental Material.

RESULTS

CIA profiles show increases from long-term averages of ~70 in the Bowen Basin and ~75 in the Sydney Basin to 80–85 regionally (Fig. 2), suggesting an increase in LSTs from 12–14 °C in QLD and 14–16 °C in NSW to 20–21 °C through the latter half of the Changhsingian. In the Bowen Basin, the transition begins above the top of the Kaloola Member of the Bandanna

[1]Supplemental Material. Data and detailed methods. Please visit https://doi.org/10.1130/GEOL.S.14524272 to access the supplemental material, and contact editing@geosociety.org with any questions.

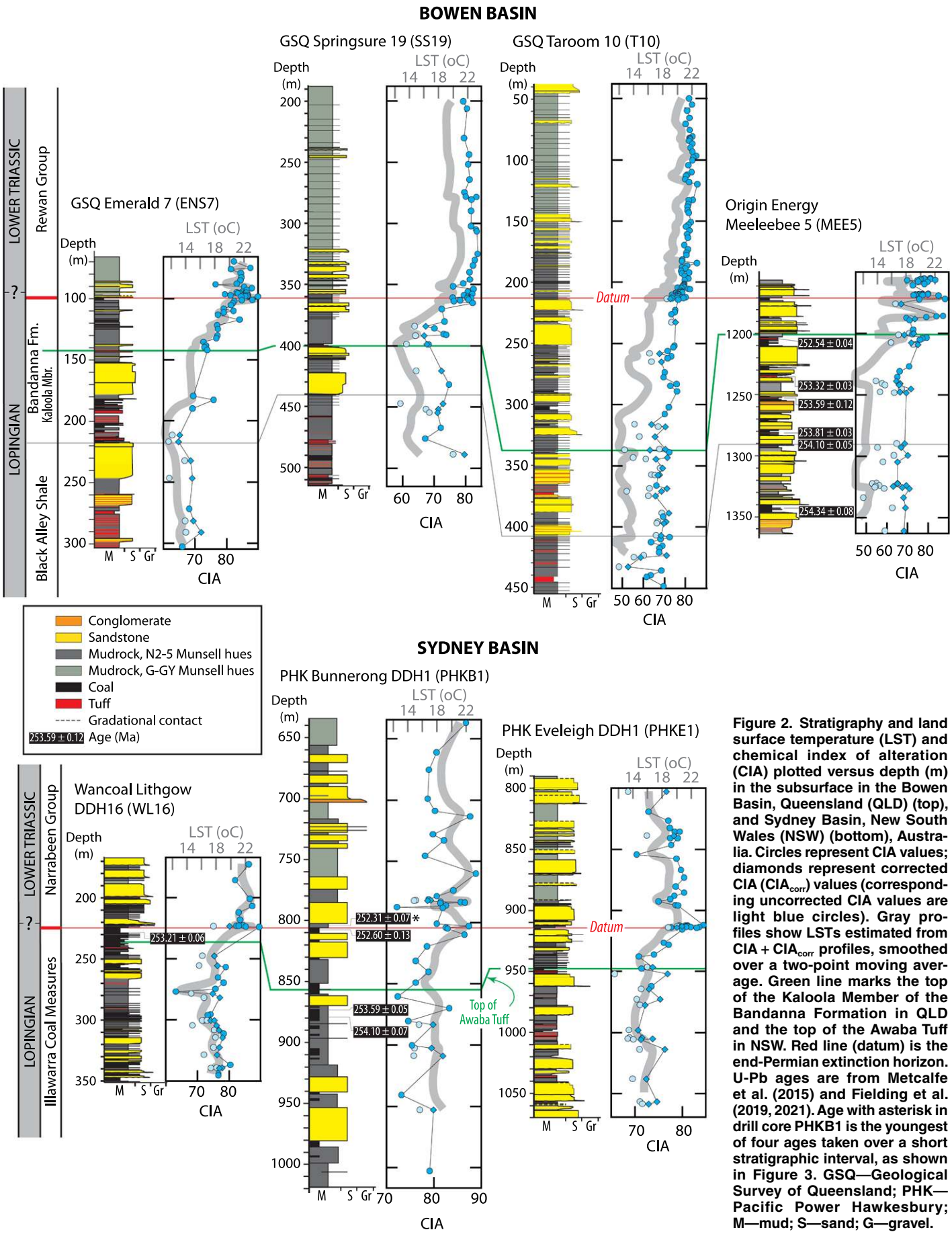

Figure 2. Stratigraphy and land surface temperature (LST) and chemical index of alteration (CIA) plotted versus depth (m) in the subsurface in the Bowen Basin, Queensland (QLD) (top), and Sydney Basin, New South Wales (NSW) (bottom), Australia. Circles represent CIA values; diamonds represent corrected CIA (CIA_{corr}) values (corresponding uncorrected CIA values are light blue circles). Gray profiles show LSTs estimated from CIA + CIA_{corr} profiles, smoothed over a two-point moving average. Green line marks the top of the Kaloola Member of the Bandanna Formation in QLD and the top of the Awaba Tuff in NSW. Red line (datum) is the end-Permian extinction horizon. U-Pb ages are from Metcalfe et al. (2015) and Fielding et al. (2019, 2021). Age with asterisk in drill core PHKB1 is the youngest of four ages taken over a short stratigraphic interval, as shown in Figure 3. GSQ—Geological Survey of Queensland; PHK—Pacific Power Hawkesbury; M—mud; S—sand; G—gravel.

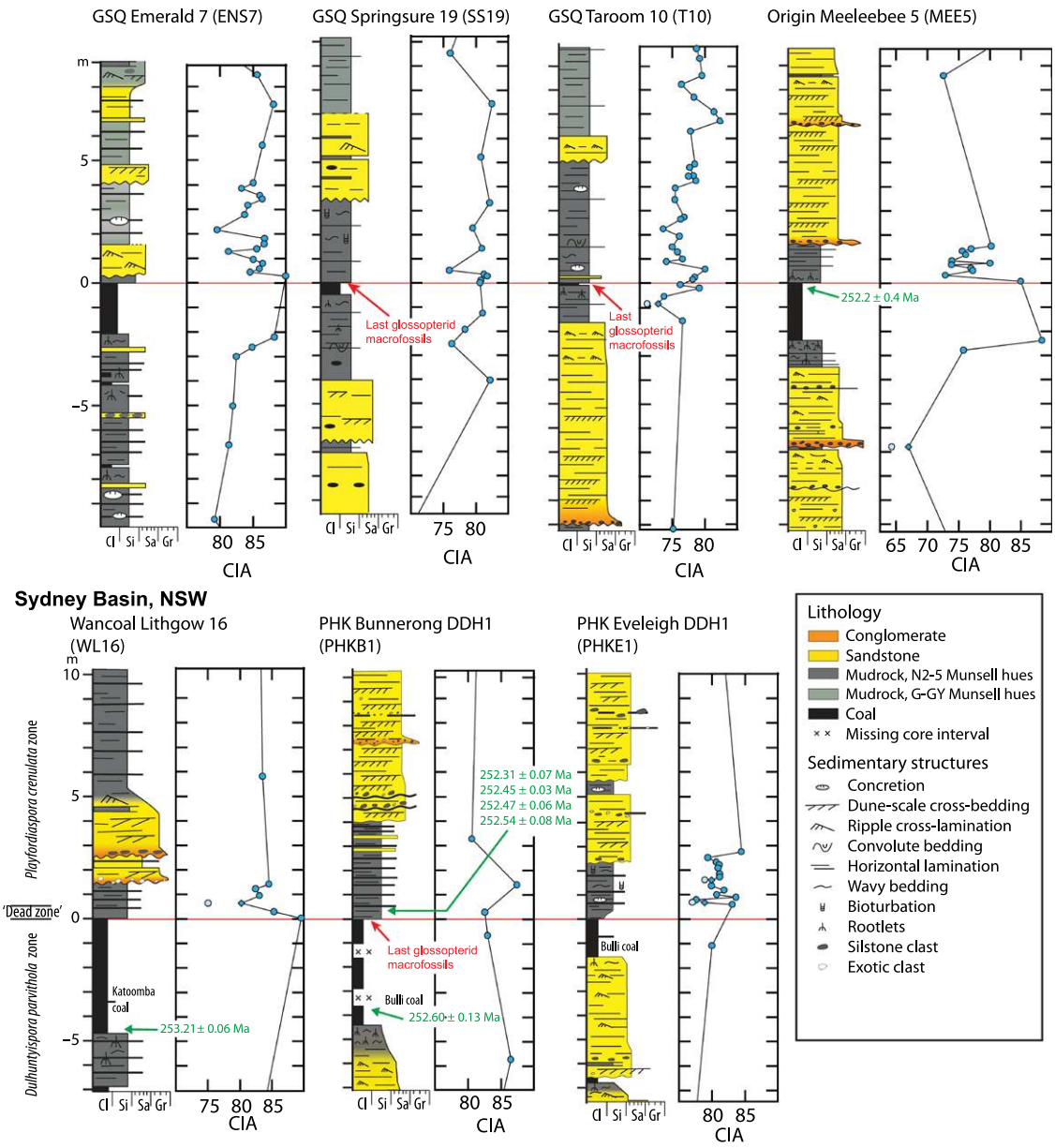

Figure 3. Detailed stratigraphy and chemical index of alteration (CIA) profiles across the end-Permian extinction (EPE) in Bowen Basin, Queensland (QLD) (top), and Sydney Basin, New South Wales (NSW) (bottom), Australia. Data plotted versus depth (m) relative to the end-Permian extinction horizon. Circles represent CIA values; diamonds represent corrected CIA values (corresponding uncorrected CIA values are light blue circles). Red line (0 m) is the EPE horizon. U-Pb ages are from Mundil et al. (2006), Fielding et al. (2019, 2021). GSQ—Geological Survey of Queensland; PHK—Pacific Power Hawkesbury. M—mud; S—sand; G—gravel.

Formation (Fig. 2), estimated at ca. 252.5 Ma in drill core MEE5 by Metcalfe et al. (2015). In the Sydney Basin, the transition begins above the Awaba Tuff, a regional marker bed, between 253.21 and 253.59 Ma (Fig. 2; Fielding et al., 2021). The EPE horizon is marked by a peak in CIA and LST values across the study area of 85–90 and 22–23 °C, respectively (Figs. 2 and 3).

CCSM3.0 simulations representing the pre-EPE latest Permian (4× pre-industrial atmospheric pCO_2 concentration) and Early Triassic (12.7× pre-industrial atmospheric pCO_2, based on the work of Kidder and Worsley [2004]) with (WP; warm poles) and without lower cloud optical depth, i.e., thinner clouds) indicate that although seasonality in SATs declined across the EPE (Fielding et al., 2019), annual average SAT rose by as much as 12–14 °C due to greenhouse forcing (Fig. 4A) and a change in cloud optical depth (Fig. 4B). Precipitation minus evaporation increased from the latest Permian to Early Triassic (Figs. 4D and 4E) due to enhanced land-sea temperature contrast, as did mid-latitude annual precipitation due to global climate shifts triggered by an increase in CO_2 radiative forcing and thinner cloud optical depth (Fig. 4F).

DISCUSSION

Changes in Weathering and LST across the EPE in Eastern Australia

The progression toward higher CIA and LST values through the upper Lopingian indicates that the entire region experienced a shift toward warmer and more humid conditions prior to the EPE (Fig. 2). Host strata are characterized by fluvial channel facies that contain indicators for extreme variability in discharge. These features, including upright, in situ stumps of trees that colonized channel floors and an abundance of sedimentary structures produced by Froude transcritical flow (Fielding et al., 2019, 2021), are common in systems affected by strong seasonality in precipitation (Fielding et al., 2018). These indicators first appear at the base of the Lopingian but increase in abundance upward through the section, suggesting that seasonality intensified in the lead-up to the EPE.

At each study site, the 5–10 m of section bracketing the EPE exhibits pronounced variability in CIA values (Fig. 3). Peak CIA values of ~83–90, which correspond to LSTs of 22–23 °C (Fig. 2), are reached at or immediately below the extinction horizon. High CIA values indicate intense chemical weathering, which could

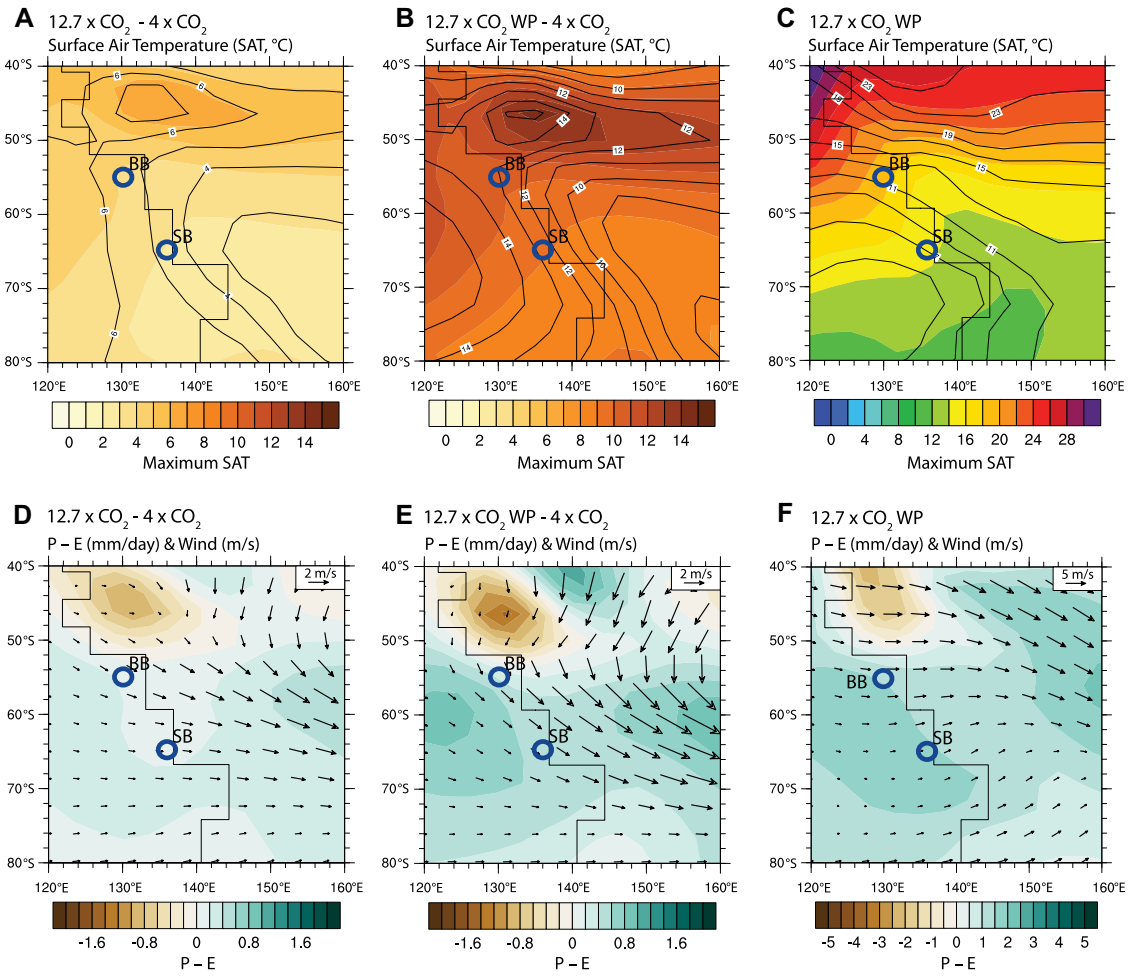

Figure 4. Community Climate System Model (CCSM3.0; https://www.cesm.ucar.edu/models/ccsm3.0/) simulations of eastern Australia at the end-Permian extinction. Upper row shows simulations for mean (contour lines, in °C) and maximum (contour shade) surface air temperature for differences between 12.7× and 4× preindustrial pCO_2 scenarios (A), differences between 12.7× pre-industrial pCO_2 simulated with warm poles (WP) due to lower cloud optical depth and 4× preindustrial pCO_2 scenarios (B), and 12.7× pre-industrial pCO_2 WP scenario. (C). Lower row (D–F) shows same but for precipitation minus evaporation (P – E; colored shading) and surface wind speed and direction (arrows). Locations of Bowen Basin (BB) and Sydney Basin (SB) are also shown.

reflect a combination of warming plus higher and possibly more intense precipitation, along with the potential corrosive effects of acid rain. At all sites except PHKB1, where the core was destructively sampled at the time of drilling, the first 0.5–1 m of post-EPE strata records an excursion to a lower CIA value (75–80) followed by a return to peak or near-peak values (Fig. 3). Throughout the BGSBS, this interval is represented by a biological "dead zone" (cf. Vajda et al., 2020), with degraded wood fragments, charcoal, and fungal spores interpreted as evidence of a deforested landscape (McLoughlin et al., 2021). Occurrences of desiccation cracks and aestivation burrows reveal evidence for groundwater-level fluctuations and the presence of wet-dry cycles, possibly including drought cycles, of unknown duration (McLoughlin et al., 2020). This interval grades upward into mudrock rich in algae and acritarchs that records groundwater ponding, interpreted as a consequence of vegetation loss (Vajda et al., 2020). Although the first traces of vascular plant recovery occur ~2 m above the EPE horizon, it is evident that landscapes remained sparsely vegetated for >3 m.y. afterward (Mays et al., 2020; Vajda et al., 2020). In this context, we interpret the excursion to low CIA values immediately above the EPE as recording a pulse of erosion associated with abrupt deforestation, which briefly exposed fresher source material characterized by lower CIA values during a time of otherwise intense chemical weathering. Given that the natural response of rivers in low-gradient settings to increased sediment load relative to water discharge is to aggrade rather than incise (Leopold et al., 1964), prolonged erosion was likely inhibited in the low-relief landscape of the BGSBS.

Above the "dead zone," geochemical profiles reveal the establishment of baseline values in CIA profiles for the Early Triassic of 80–85, corresponding to LSTs of 20–21 °C (Fig. 2). The overall decrease from peak CIA values at the EPE may reflect rebounding temperatures and/or a cessation of contributions from acid rain, but persistently higher values than typical of the Lopingian imply a permanent shift to warmer temperatures and overall higher humidity and/or seasonal precipitation. Macrofloras in this interval are indicative of at least seasonally moist conditions (McLoughlin et al., 2021). An irregular transition in mudrock coloration, from gray to G (green) or GY (green-yellow) Munsell hues that reflect the gradual development of better-drained alluvial landscapes, contrasts with the gray coloration indicative of the permanently wet conditions of the Lopingian (Fielding et al., 2019, 2021).

Simulations of Pre- and Post-EPE Climate in Eastern Australia

Climate simulations cannot reconstruct the level of spatiotemporal detail preserved in the stratigraphic succession. However, model results are consistent with a scenario involving intense warming and overall higher but more seasonal precipitation in response to the combined effect of high CO_2 radiative forcing and thinner clouds. Although seasonality in SAT apparently decreased, especially over land (Fig. 4B), the climate was much warmer overall, with SATs along the continental margin ~12–14 °C higher in the Early Triassic than in the latest Permian (Fig. 4C).

Synthesis and Implications

Our data and model-based estimates of 10–14 °C warming are consistent with published estimates, all derived from paleotropical latitudes, which indicate that temperature rose by as much as 15 °C across the EPE (Joachimski et al., 2012). Our estimated temperature maximum of 22–23 °C is remarkably high given the paleolatitude of the BGSBS. However, when considered in the context of estimated temperature

maxima for the paleotropics of >35 °C (Sun et al., 2012), our results imply a modest flattening of the paleolatitudinal temperature gradient at the time of the EPE. Although temperatures in eastern Australia subsequently declined by a few degrees, the sharp rise across the EPE, combined with other factors, likely crossed an intolerable threshold for long-established temperate-zone forest-mire communities.

A global expansion of arid zones across the EPE has been inferred by previous workers (Chumakov and Zharkov, 2003; Benton and Newell, 2014), but this signal is not apparent in eastern Australia. Although coal deposition ceased, there is no evidence for immediate aridification across the EPE in the BGSBS. Indeed, retention of higher moisture levels along this continental margin likely provided key refugia for moisture-loving terrestrial groups that survived the EPE (McLoughlin et al., 2021).

CONCUSIONS

In eastern Australia, *Glossopteris* forest-mire ecosystems thrived through the Lopingian, a time of gradual warming and increasingly seasonal climate. The terrestrial crisis coincided with an episode of intense chemical weathering, peak warmth, and associated environmental stresses that crossed a tolerance threshold for floral ecosystems. Prolonged erosion following vegetation collapse was limited in what was a low-gradient landscape. Although the post-EPE climate was 10–14 °C warmer and landscapes were no longer persistently wet, our results point to overall higher but more seasonal precipitation consistent with an intensification of a monsoonal climate regime in southeastern Gondwana.

ACKNOWLEDGMENTS

This research was funded by U.S. National Science Foundation (NSF) grants EAR-1636625 (C.R. Fielding and D. Frank) and EAR-1636629 (A.M.E. Winguth and C. Winguth), Swedish Research Council VR grants 2019-4061 (V. Vajda) and 2014-5234 and 2018-04527 (S. McLoughlin), and the Royal Swedish Academy of Sciences. We acknowledge NSF-sponsored high-performance computing support from Cheyenne (https://doi.org/10.5065/D6RX99HX) provided by the U.S. National Center for Atmospheric Research (NCAR) Computational and Information Systems Laboratory. We thank reviewers D. Chu, R. Gastaldo, and S. Bourquin for comments and insights that improved the manuscript.

REFERENCES CITED

Algeo, T.J., and Twitchett, R.J., 2010, Anomalous Early Triassic sedimentary fluxes due to elevated weathering rates and their biological consequences: Geology, v. 38, p. 1023–1026, https://doi.org/10.1130/G31203.1.

Benton, M.J., and Newell, A.J., 2014, Impacts of global warming on Permo-Triassic terrestrial ecosystems: Gondwana Research, v. 25, p. 1308–1337, https://doi.org/10.1016/j.gr.2012.12.010.

Burgess, S.D., Muirhead, J.D., and Bowring, S.A., 2017, Initial pulse of Siberian Traps sills as the trigger of the end-Permian mass extinction: Nature Communications, v. 8, 164, https://doi.org/10.1038/s41467-017-00083-9.

Cao, Y., Song, H., Algeo, T.J., Chu, D., Du, Y., Tian, L., Wang, Y., and Tong, J., 2019, Intensified chemical weathering during the Permian-Triassic transition recorded in terrestrial and marine successions: Palaeogeography, Palaeoclimatology, Palaeoecology, v. 519, p. 166–177, https://doi.org/10.1016/j.palaeo.2018.06.012.

Chumakov, N.M., and Zharkov, M.A., 2003, Climate during the Permian–Triassic biosphere reorganizations: Article 2. Climate of the Late Permian and Early Triassic: General inferences: Stratigraphy and Geological Correlation, v. 11, p. 361–375.

Collins, W.D., et al., 2006, The Community Climate System Model version 3 (CCSM3): Journal of Climate, v. 19, p. 2122–2143, https://doi.org/10.1175/JCLI3761.1.

Fielding, C.R., Alexander, J., and Allen, J.A., 2018, The role of discharge variability in the formation and preservation of alluvial sediment bodies: Sedimentary Geology, v. 365, p. 1–20, https://doi.org/10.1016/j.sedgeo.2017.12.022.

Fielding, C.R., et al., 2019, Age and pattern of the southern high-latitude continental end-Permian extinction constrained by multiproxy analysis: Nature Communications, v. 10, 385, https://doi.org/10.1038/s41467-018-07934-z.

Fielding, C.R., Frank, T.D., Tevyaw, A.P., Savatic, K., Vajda, V., McLoughlin, S., Mays, C., Nicoll, R.S., Bocking, M., and Crowley, J.L., 2021, Sedimentology of the continental end-Permian extinction event in the Sydney Basin, eastern Australia: Sedimentology, v. 68, p. 30–62, https://doi.org/10.1111/sed.12782.

Holcombe, R.J., Stephens, C.J., Fielding, C.R., Gust, D.A., Little, T.A., Sliwa, R., Kassan, J., McPhie, J., and Ewart, A., 1997, Tectonic evolution of the northern New England Fold Belt: The Permian-Triassic Hunter-Bowen event, *in* Ashley, P.M., and Flood, P.G., eds., Tectonics and Metallogenesis of the New England Orogen: Geological Society of Australia Special Publication 19, p. 52–65.

Joachimski, M.M., Lai, X., Shen, S., Jiang, H., Luo, G., Chen, B., Chen, J., and Sun, Y., 2012, Climate warming in the latest Permian and the Permian–Triassic mass extinction: Geology, v. 40, p. 195–198, https://doi.org/10.1130/G32707.1.

Kaiho, K., et al., 2016, Effects of soil erosion and anoxic-euxinic ocean in the Permian-Triassic marine crisis: Heliyon, v. 2, e00137, https://doi.org/10.1016/j.heliyon.2016.e00137.

Kidder, D.L., and Worsley, T.R., 2004, Causes and consequences of extreme Permo-Triassic warming to globally equable climate and relation to the Permo-Triassic extinction and recovery: Palaeogeography, Palaeoclimatology, Palaeoecology, v. 203, p. 207–237, https://doi.org/10.1016/S0031-0182(03)00667-9.

Knoll, A.H., Bambach, R.K., Payne, J.L., Pruss, S., and Fischer, W.W., 2007, Paleophysiology and end-Permian mass extinction: Earth and Planetary Science Letters, v. 256, p. 295–313, https://doi.org/10.1016/j.epsl.2007.02.018.

Kump, L.R., Pavlov, A., and Arthur, M.A., 2005, Massive release of hydrogen sulfide to the surface ocean and atmosphere during intervals of oceanic anoxia: Geology, v. 33, p. 397–400, https://doi.org/10.1130/G21295.1.

Leopold, L.B., Wolman, M.G., and Miller, J.P., 1964, Fluvial Processes in Geomorphology: San Francisco, W.H. Freeman, 522 p.

Li, C., and Yang, S., 2010, Is chemical index of alteration (CIA) a reliable proxy for chemical weathering in global drainage basins?: American Journal of Science, v. 310, p. 111–127, https://doi.org/10.2475/02.2010.03.

Martini, I.P., and Chesworth, W., 2013, Weathering, Soils and Paleosols: Amsterdam, Elsevier, 618 p.

Mays, C., Vajda, V., Frank, T.D., Fielding, C.R., Nicoll, R.S., Tevyaw, A.P., and McLoughlin, S., 2020, Refined Permian–Triassic floristic timeline reveals early collapse and delayed recovery of south polar terrestrial ecosystems: Geological Society of America Bulletin, v. 132, p. 1489–1513, https://doi.org/10.1130/B35355.1.

McKellar, J.L., 1977, Palynostratigraphy of samples from GSQ Taroom 10: Queensland Government Mining Journal, v. 78, p. 579–584.

McLoughlin, S., Mays, S., Vajda, V., Bocking, M., Frank, T.D., and Fielding, C.R., 2020, Dwelling in the dead zone—Vertebrate burrows immediately succeeding the end-Permian extinction event in Australia: Palaios, v. 35, p. 342–357, https://doi.org/10.2110/palo.2020.007.

McLoughlin, S., Nicoll, R.S., Crowley, J.L., Vajda, V., Mays, C., Fielding, C.R., Frank, T.D., Wheeler, A., and Bocking, M., 2021, Age and paleoenvironmental significance of the Frazer Beach Member—A new lithostratigraphic unit overlying the end-Permian extinction horizon in the Sydney Basin, Australia: Frontiers in Earth Sciences, v. 8, 600976, https://doi.org/10.3389/feart.2020.600976.

Metcalfe, I., Crowley, J.L., Nicoll, R.S., and Schmitz, M., 2015, High-precision U-Pb CA-TIMS calibration of Middle Permian to Lower Triassic sequences, mass extinction and extreme climate-change in eastern Australian Gondwana: Gondwana Research, v. 28, p. 61–81, https://doi.org/10.1016/j.gr.2014.09.002.

Michaelsen, P., 2002, Mass extinction of peat-forming plants and the effect on fluvial styles across the Permian-Triassic boundary, northern Bowen Basin, Australia: Palaeogeography, Palaeoclimatology, Palaeoecology, v. 179, p. 173–188, https://doi.org/10.1016/S0031-0182(01)00413-8.

Mundil, R., Metcalfe, I., Chang, S., and Renne, P.R., 2006, The Permian-Triassic boundary in Australia: New radio-isotope ages: Geochimica et Cosmochimica Acta, v. 70, Supplement, p. A 436, https://doi.org/10.1016/j.gca.2006.06.876.

Nesbitt, H.W., and Young, G.M., 1982, Early Proterozoic climates and plate motion inferred from major element chemistry of lutites: Nature, v. 299, p. 715–717, https://doi.org/10.1038/299715a0.

Panahi, A., Young, G.M., and Rainbird, R.H., 2000, Behavior of major and trace elements (including REE) during Paleoproterozoic pedogenesis and diagenetic alteration of an Archean granite near Ville Marie, Québec, Canada: Geochimica et Cosmochimica Acta, v. 64, p. 2199–2220, https://doi.org/10.1016/S0016-7037(99)00420-2.

Retallack, G.J., and Jahren, A.H., 2008, Methane release from igneous intrusion of coal during Late Permian extinction events: The Journal of Geology, v. 116, p. 1–20, https://doi.org/10.1086/524120.

Riccardi, A., Kump, L.R., Arthur, M.A., and D'Hondt, S., 2007, Carbon isotopic evidence for chemocline upward excursions during the end-Permian event: Palaeogeography, Palaeoclimatology, Palaeoecology, v. 248, p. 73–81, https://doi.org/10.1016/j.palaeo.2006.11.010.

Sun, H., Xiao, Y., Gao, Y., Zhang, G., Casey, J.F., and Shen, Y., 2018, Rapid enhancement of chemical weathering recorded by extremely light seawater lithium isotopes at the Permian-Triassic boundary: Proceedings of the National Academy of Sciences of the United States of America, v. 115, p. 3782–3787, https://doi.org/10.1073/pnas.1711862115.

Sun, Y., Joachimski, M.M., Wignall, P.B., Yan, C., Chen, Y., Jiang, H., Wang, L., and Lai, X., 2012, Lethally hot temperatures during the Early Triassic greenhouse: Science, v. 338, p. 366–370, https://doi.org/10.1126/science.1224126.

Vajda, V., McLoughlin, S., Mays, C., Frank, T.D., Fielding, C.R., Tevyaw, A., Lehsten, V., Bocking, M., and Nicoll, R.S., 2020, End-Permian (252 Mya) deforestation, wildfires and flooding—An ancient biotic crisis with lessons for the present: Earth and Planetary Science Letters, v. 529, 115875, https://doi.org/10.1016/j.epsl.2019.115875.

Wignall, P.B., 2015, The Worst of Times: How Life on Earth Survived Eighty Million Years of Extinction: Princeton, New Jersey, Princeton University Press, 224 p.

Wignall, P.B., and Twitchett, R.J., 1996, Oceanic anoxia and the end Permian mass extinction: Science, v. 272, p. 1155–1158, https://doi.org/10.1126/science.272.5265.1155.

Winguth, A.M.E., Shields, C.A., and Winguth, C., 2015, Transition into a hothouse world at the Permian-Triassic boundary—A model study: Palaeogeography, Palaeoclimatology, Palaeoecology, v. 440, p. 316–327, https://doi.org/10.1016/j.palaeo.2015.09.008.

Yang, J., Cawood, P.A., Du, Y., Feng, B., and Yan, J., 2014, Global continental weathering trends across the Early Permian glacial to postglacial transition: Correlating high- and low-paleolatitude sedimentary records: Geology, v. 42, p. 835–838, https://doi.org/10.1130/G35892.1.

Printed in USA